Remote Sensing Applications: Society and Environment
November 2024, Volume 36 Pages 101340 (15p.)
https://doi.org/10.1016/j.rsase.2024.101340
https://archimer.ifremer.fr/doc/00905/101643/

Spatial variability of temperature inside atoll lagoons assessed with Landsat-8 satellite imagery

Van Wynsberge Simon [1, 2, *], Quere Robin [1], Andréfouët Serge [3], Autret Emmanuelle [4], Le Gendre Romain [1]

[1] Institut Français de Recherche pour l'Exploitation de la Mer, UMR 9220 ENTROPIE (Institut de Recherche pour le Développement, Université de la Réunion, Ifremer, Université de la Nouvelle-Calédonie, Centre National de la Recherche Scientifique), Nouméa, 98 800, New Caledonia
[2] Ifremer, IRD, ILM, UPF, UMR 241 SECOPOL, Vairao, 98725, Tahiti, French Polynesia
[3] Institut de Recherche pour le Développement, UMR 9220 ENTROPIE (Institut de Recherche pour le Développement, Université de la Réunion, Ifremer, Université de la Nouvelle-Calédonie, Centre National de la Recherche Scientifique), Vairao, 98725, Tahiti, French Polynesia
[4] fremer, Univ. Brest, CNRS, IRD, Laboratoire d'Océanographie Physique et Spatiale (LOPS), IUEM, Brest, France

* Corresponding author : Simon Van Wynsberge, email address : simon.van.wynsberge@ifremer.fr

Abstract :

Sea Surface Temperature (SST) maps are necessary for managing marine resources in a climate change context, but are lacking for most of the 598 world's atolls. We assessed the feasibility of using the Landsat-8 (L8) satellite to infer SST maps for four French Polynesia atolls of aquaculture interest in Tuamotu Archipelago, namely Takaroa, Raroia, Tatakoto, and Reao. Specifically, we (1) used sensors to measure in situ the range of spatial temperature differences recorded in these four atoll lagoons; (2) calibrated and assessed the performances of SST algorithms to estimate lagoon temperature from L8 signals; (3) generated temperature maps for the lagoons and compared spatial patterns of temperature obtained from these maps with patterns highlighted by in situ sensors. Good agreements between satellite and in situ temperature data were obtained, with better results achieved when using an atoll-by-atoll optimization (average bias = −0.26 °C; RMSE = 0.55 °C). However, we also show that the range of temperature inside atoll lagoons is low, and of the same order of magnitude than RMSE achieved with SST algorithms. Because of the L8 overpass time (~9 a.m.) and the revisit time (16 days), L8 SST could not capture the entire range of spatial differences measured in situ in the four lagoons, but could capture spatial gradients and fronts better than with few in situ sensors. Considering the achieved accuracies and the actual temperature differences at the four study sites, we discuss the usefulness of L8 derived SST maps to assist fishery and aquaculture management in atoll lagoons, as well as the possible generalization to other lagoons.

Highlights

► Landsat SST and *in situ* temperature are in good agreement in four atoll lagoons. ► Landsat captured SST spatial gradients much better than sparse *in situ* loggers. ► Landsat products can serve physical models, sampling strategy, and spatial planning.

Keywords : Landsat, Sea surface temperature, Coral reefs, Aquaculture, Fisheries

1. Introduction

Sea surface temperature (SST) is a fundamental variable for understanding physical and biological processes and informing management (O'carroll *et al.*, 2019 ; Melet *et al.*, 2020). In the context of global warming, mapping temperature is necessary information for managing marine environments and resources on the long run, for instance to inform aquaculture site selection (Palmer *et al.*, 2020), identify temperature fronts of ecological and fishery relevance (Belkin *et al.*, 2021), delimiting the productive habitats of exploited wild stocks (Klemas, 2013), mapping refugia and areas of high mortality risk for important species (Eladawy *et al.*, 2022), or informing marine spatial planning scenarios (Petrosillo *et al.*, 2023).

In the Pacific Ocean, atoll lagoons are home to activities dependent on a variety of wild marine resources (e.g., mariculture, fishing). The sustainability of these activities is in particular challenged by global warming and episodes of marine heat waves (Bell *et al.*, 2011; Andréfouët *et al.*, 2018). In these ecosystems, temperature can vary substantially at scales < 100 m between geomorphological zones, due to the differences in heat fluxes at the atmosphere-water interface, differences in substrate composition and depth which affect or amplify fluxes through their albedo, and the advection powered by tide and wave-driven currents (McCabe *et al.*, 2010; Grimaldi *et al.*, 2023). Notably in small and enclosed atoll lagoons, the combined effect of these factors can deviate significantly lagoon temperature from the surrounding ocean (Van Wynsberge *et al.*, 2017).

In the Tuamotu archipelago, French Polynesia, maps of temperature inside lagoons have been produced by spatial interpolation or modelling, but only for a couple of atolls, mainly to inform temperature-dependant biological models (Dumas *et al.*, 2012; Thomas *et al.*, 2016). However, spatially-explicit temperature products representative of thermal conditions experienced by marine resources are requested by local managers to identify the most suitable areas for safely rearing aquaculture species and plan for the conservation of important species.

Recording temperature data in a spatially explicit manner using *in situ* sensors is possible but costly and complicated in remote and difficult-to-access lagoons owing in particular to the necessary periodic visits for logger maintenance. As a result, *in situ* sensors can be used to measure temperature at specific locations, but can rarely be deployed in sufficient numbers and over sufficiently long periods to characterize the diversity of thermal habitats in space (longitude, latitude, depth) and time (but see Grimaldi *et al.*, 2023 or Bruyère *et al.*, 2023a; Bruyère *et al.*, 2024). These scattered *in situ* measurements can provide time series at specific points, but cannot offer a spatially continuous view with precise information on temperature fronts at an appropriate resolution (< 1km). The use of high-resolution 3D hydrodynamic models for lagoons can produce precise temperature maps at high temporal resolution (Dumas *et al.*, 2012), but setting up such models is complex and, besides the bathymetry, they also require a number of calibration/validation *in situ* data also difficult to acquire in remote atolls (Dumas *et al.*, 2012, Andréfouët *et al.*, 2023, Bruyère *et al.*, 2023a; 2023b; 2024). As a result, 3D hydrodynamical models are available only for four French Polynesia lagoons to date (Ahe,

Takaroa, Raroia and Gambier) and cannot be used routinely to generate temperature products elsewhere for every exploited lagoons. On the other hand, daily SST remote sensing Level-4 products deliver gridded SST data at global (e.g., OSTIA; MUR; G1SST; see Dash *et al.*, 2012 for a review) or regional (e.g. RAMSSA; Beggs *et al.*, 2011) scales. One-kilometre-resolution satellite-derived SST data from various instruments, such as Moderate-Resolution Imaging Spectroradiometer (MODIS) and Advanced Very-High-Resolution radiometer (AVHRR) are ingested by these Level-4 SST products. Assuming some validation and correction are applied (Van Wynsberge *et al.*, 2017 ; Van Wynsberge *et al.*, 2020 ; Grimaldi *et al.*, 2023), these products can be helpful for studying lagoon temperature. However, due to resampling and interpolation methods, the true resolution is lower (Chin *et al*., 2017) and appears inadequate for many lagoons. Swath Level-1 1km SST products from infrared sensors does not suffer from aggregation or interpolation smoothing, but their resolution is too coarse to capture fine scale patterns in the very nearshore areas and are not adequate for small closed or semi-closed water bodies due to the proximity of land. In order to fill these gaps, a suitable candidate is the Landsat Mission run by the Earth Observation Program of the National Aeronautics and Space Administration (NASA) and by the United States Geological Survey (USGS), from Landsat-4 (1982-1993) to Landsat-8 (L8; 2013 to present) (Xing *et al.*, 2006; Baughman & Conaway, 2021).

L8 satellite images have shown good results for mapping SST at fine scale in coastal environments open to the ocean (Syariz *et al.*, 2015; Jang and Park, 2019; Susilo *et al.*, 2019;

Vanhellemont, 2020; Vanhellemont *et al.*, 2022; Bradtke, 2021) as well as bays, channels, estuaries (Wang *et al*., 2016; Snyder *et al.*, 2017; Trinh *et al.*, 2017; Mondejar and Tongco, 2019), macrotidal flats (Lee *et al.*, 2022), and rivers (Baughman & Conaway, 2021). The L8 infrared spectral bands 10 (11 µm) and 11 (12 µm) can provide SST with a spatial resolution of 100m (resampled at 30m in the delivered product) and a revisit time of 16 days. The process requires the calibration of an empirical relationship between temperature recorded in the field and the Bands 11 and 12 infrared signals, sometimes coupled with large-scale daily SST products (Minnett *et al.*, 2019; Jang & Park, 2019). However, the errors associated to these SST estimates vary greatly in the literature, from a RMSE lower than 0.03°C for a case study based on a single image in Indonesia (Syariz *et al.*, 2015) to 2.25°C for an Alaska river studied with numerous images (Baughman & Conaway, 2021). The identified factors that influence the accuracy of SST retrievals include the type of algorithms and the methods used for their optimisation, but also the environmental conditions or site-specific parameters at the time of image acquisition (e.g., cloud cover, wind speed, as discussed in Jang and Park, 2019).

For atolls and their lagoon environments, the ability of SST algorithms to represent temperature accurately enough to be useful for marine resource management remains unclear. Indeed, atoll lagoons have a number of specific features that can affect the retrieval of accurate SST using L8 images. First, atoll lagoons are usually dotted by small emerged and intertidal structures (e.g., lagoon pinnacles and patch reefs, Andréfouët *et al.*, 2020) that may impact an accurate retrieval. Second, temperature variation in atoll lagoons are strongly dependent on

geomorphology, lagoon shapes, and their degree of local confinement, so that temperature high and lows are often encountered on lagoon extremities that are typically more confined. Also, temperature gradients are more pronounced when approaching atoll passes and shallow channels where tide or wave-driven inflows of ocean water occur. However, inside the French Polynesia lagoons, the reported horizontal temperature variability at any given moment is generally of the order of less than one degree at most (Dumas *et al.*, 2012; Bruyère *et al.*, 2023a), hence much lower than the range reported in most other L8 derived SST studies (Jang and Park, 2019; Vanhellemont, 2020; Bradtke, 2021; Wang *et al.*, 2016; Snyder *et al.*, 2017; Lee *et al.*, 2022; Baughman & Conaway, 2021; Twumasi *et al.*, 2021). On the other hand, clouds might be less problematic above Tuamotu atoll lagoons compared to high islands owing to the low topography of atolls (Barnes *et al.*, 2016), which could be an advantage for SST mapping by remote sensing.

With all the aforementioned constraints and features in mind, we aim here to : (1) use *in situ* sensors to measure *in situ* the range of spatial temperature differences recorded in four atoll lagoons of aquaculture interest in French Polynesia; (2) calibrate and assess the performances of SST algorithms to estimate lagoon temperature from L8 infrared signals; (3) generate temperature maps for the lagoons and compare spatial patterns of temperature obtained from these maps with patterns highlighted by *in situ* sensors. Finally, considering the achieved accuracies and the actual temperature differences at the four study sites, we discuss the

usefulness of L8 derived SST maps to assist fishery and aquaculture management in atoll lagoons, as well as possible generalization to other lagoons.

2. Material and methods

2.1 Study sites

The Tuamotu archipelago, French Polynesia, includes one tenth of the 598 world's atolls (Andréfouët and Paul, 2023). Seasonal variability of temperature is low in this archipelago, with oceanic SST ranging from 25°C in August to 29°C in March (monthly climatology values, Heron *et al.*, 2015). Temperature inside atoll lagoons may display a higher seasonal variability depending on lagoon geomorphology and water renewal (Van Wynsberge *et al.*, 2017; 2020). Oceanic tidal variation is also low in the Tuamotu archipelago (maximum level variation < 1 m during spring tide, and 20-30 cm in mean; Aucan *et al.*, 2021; Van Wynsberge *et al.*, 2017). Tidal range inside semi-closed to semi-open lagoons is even lower than oceanic tidal range due to the limited apertures allowing water transfer between ocean and lagoon (Aucan *et al.*, 2021). Beyond the effect of tide, water level inside atoll lagoons may rise or fall depending on offshore wave conditions, but variations in lagoon water level typically remain below 1 m (i.e.: Varillon *et al.*, 2019; Aucan *et al.*, 2021; Andréfouët *et al.*, 2023), except during the strongest swell events (Canavesio, 2019). In terms of wind regimes at the scale of the archipelago, moderate eastern winds (4.4 m s^{-1} in average) dominate all year long, but low wind from the North-East

occur during the warm season, as well as strong wind from East-South-East (6.3 m s^{-1}) during the cool period (Dutheil *et al.*, 2020).

This study focuses on four atoll lagoons which are of aquaculture interest in the Tuamotu archipelago, namely Tatakoto, Reao, Takaroa, and Raroia (Fig. 1). Spat collection and rearing of the giant clam (*Tridacna maxima*) take place in Tatakoto and Reao (Wabnitz & Remoissenet, 2012), but these activities have been affected by bleaching events in 2016 and 2017 triggered by unusually high SST (Andréfouët *et al.*, 2018). Takaroa and Raroia are two black pearl-farming lagoons, based on spat collection, grafting and rearing of the black-lipped oyster *Pinctada margaritifera*. This lucrative activity has collapsed in Takaroa following a dystrophy phenomenon that occurred in 2013 (Rodier *et al.*, 2019). Nevertheless, this atoll remains of high interest to monitor its recovery (Monaco *et al.*, 2021), as atolls have shown variations of their pearl farming potential at decadal scales.

The rim surrounding the lagoons of Tatakoto (11.46 km^2) and Reao (44.1 km^2) are closed by land in their northern parts, but exchanges between lagoon water and the ocean are possible through shallow channels (locally called *hoa*) that segment the southern part of their rim. These two atolls can be qualified as semi-closed atolls. Reao is made of three lagoonal basins which get larger from north to south. Takaroa lagoon (90 km^2) is considered semi-open due to a narrow but deep pass and the presence of *hoa* on both northwest and south sections of the rim. Finally, Raroia lagoon is the largest of our study sites (359 km^2) and the more open to ocean due to the presence of a deep pass and a rim segmented by numerous *hoa*, including a very wide one in

the south (Aucan *et al.*, 2021). The maximum depth are 68 m and 48 m, respectively for Raroia and Takaroa (Andréfouët *et al.*, 2020), and 32 m in Reao (unpublished data), and probably < 30 m at Tatakoto, although not yet quantified.

2.2 In situ temperature data

Lagoon temperatures were recorded every 10 to 60 minutes with good accuracy (< 0.05 °C) and stability using 16 loggers (TWR2050, Duet, and Duo from RBR®; SBE56 from Seabird Scientific®; Sambat from NKE instrumentation®) deployed at certain period during the 2012-2023 period, at Tatakoto (n = 3), Takaroa (n = 4), Raroia (n = 5), and Reao (n = 10; Fig. 1; Table 1). All loggers were deployed between 1 and 4 m depth, and were preferentially deployed in areas exposed to distinct thermal regimes inside lagoons owing to previous knowledge (Takaroa, Tatakoto) or they were deployed as systematically as possible to capture this variability (Raroia, Reao; Fig. 1). Having sensors located at slightly different depths below the air-water interface (1-4 m depth) was deemed adequate in the context of this study because vertical stratification of temperature in these lagoons is null or negligible at the hours of L8 overpass (i.e., between 09:07 AM and 09:45 AM depending on atolls; Fig. A7 and A8). Moreover, temperature at 1-4 m depth is more representative of the conditions experienced by exploited organisms than skin-temperature, and is therefore more relevant for fisheries and aquaculture applications.

At Tatakoto, TAT1 and TAT2 loggers were located in the West and East extremities of the lagoon respectively, while the third logger (TAT3) was located in the southern inner slope.

At Takaroa, TAK1 and TAK3 were both located on the South-West inner slope of the rim, whereas TAK2 was located near the narrow pass and TAK4 on a lagoon patch reef near the lagoon center.

At Raroia, RAR7 and RAR8 were located on patch reefs at proximity of the inner slope, while RAR4, RAR5, and RAR6 were located on central lagoon patch reefs, respectively located in the North, middle, and South parts of the lagoon. Deployments at Raroia were performed at three different depths before, during, and after the MALIS 1 and 2 oceanographic cruises (Andréfouët, 2018, Bruyère *et al.*, 2023a), but only those between 1.5m and 2.5m were used for this study.

Finally, at Reao, the sampling strategy was more extensive and could cover lagoon patch reefs located in the north, middle, and south part of the lagoon (REA10, REA11 REA2, REA1, REA9, REA5 and REA4), the inner slope of the emerged rim (REA8), the reef flats of the open rim (REA7), and the shallow sandy terrace located near the closed rim (REA6).

We defined as "positive gradient in the lagoon length" an increasing temperature (difference in hourly mean temperature $\geq 0.1°C$) recorded between RAR4, RAR5 and RAR6 at Raroia, between TAK1 and TAK3 at Takaroa, between REA2, REA9 and REA5 at Reao, and between TAT2, TAT3 and TAT1 at Tatakoto, and *vice versa* for negative gradients. In the lagoons' width axis, we defined as "positive gradient" an increasing temperature (difference in hourly mean temperature $\geq 0.1°C$) recorded between RAR8, RAR6 and RAR7 at Raroia, between

REA11 and REA10 at Reao, and between TAK1 and TAK2 at Takaroa, and *vice versa* for negative gradients.

2.3 Regional satellite SST data

In addition to *in situ* data, daily temperature estimates from regional SST analysis were required to calibrate the SST algorithm tested in this study (see section 2.5). For this, SST fields with a coarse resolution can be used. Specifically, the Multi-scale Ultra-high-Resolution Sea Surface Temperature product (MUR-SST), which provides daily SST at 0.01 degree (around 1 km) spatial resolution (Chin *et al.*, 2017; https://podaac.jpl.nasa.gov/dataset/MUR-JPL-L4-GLOB-v4.1) was chosen since a previous study demonstrated its good performance for estimating SST at lagoon scale in Raroia (Van Wynsberge *et al.*, 2020). The MUR-SST data were extracted for the geographic positions of each temperature logger (Table 1).

2.4 Landsat satellite imagery and thermal band quality-control

Level 1 Collection 2 images from the L8 Operational Land Imager and Thermal Infrared Sensor (OLI/TIRS; https://doi.org/10.5066/P975CC9B) that matched the dates of *in situ* measurements of temperature were downloaded using Google Earth Engine® (n = 237 images, all atolls included). This platform automatizes the download of a collection of cropped images, while maintaining the original projection, resolution and digitization resolution, here at 16 bits (Gorelick *et al.*, 2017). L8 satellite data were always acquired between 9:07 and 09:45 local time at the four study sites, and "matchups" between images and *in situ* data were defined by

associating images to the nearest (< 1 hr) measurement. A “matchup” is hereafter defined as a couple of one *in situ* data and its concurrent L8 measurement. Hence, for a given L8 image, if five sensors provide ±1 hour concurrent *in situ* data, then a total of five matchups are theoretically available.

Thermal infrared bands 10 (11 µm) and 11 (12 µm), provided at 30 m resolution by United States Geological Survey (USGS), were extracted for each image. Note that these bands are initially recorded at 100 m resolution by TIRS, but resampled at 30 m resolution on the OLI grid and orthorectified during the Level 1 image processing (Vanhellemont *et al.*, 2022). To compare the thermal infrared band with *in situ* temperature data (section 2.5), only the L8 pixels intersecting the *in situ* data positions were used. This procedure was supported by a sensitivity analysis that compared the agreement between both data sets while changing the window size considered to extract satellite data around the *in situ* sensor positions (Fig. A1).

Based on the Quality Assessment (QA) band, only the valid pixels of bands 10 (DN_{10}) and 11 (DN_{11}) were kept. This quality band identifies pixels contaminated by clouds, cloud shadows, and emerged vegetation. To avoid problems potentially due to pixel coregistration uncertainty (1 pixel), a 1-pixel (30 m)-buffer was further added to the QA-masked areas. However, since the QA Pixel field provided by USGS was found to be insufficiently stringent for our SST application, and because stripping patterns in the along-track direction affected images due to a TIRS detector-to-detector mis-calibration (Stumpf *et al.*, 2018; https://earth.esa.int/eogateway/instruments/tirs/quality-control-reports/products-anomalies), a

manual image-by-image control was carried out to check pixel quality around the *in situ* sensors. Specifically, matchups between satellite and *in situ* data were retained to inform the SST-algorithm-optimization protocol (section 2.5) only if i) no cloud could be visually detected in a 20 pixels buffer surrounding the *in situ* sensor position, ii) no cirrus, as detected by band 9 following Skakun *et al.* (2022), affected the pixel at sensor position, and iii) no visually detectable strips overlapped the *in situ* sensor. Image stripping detection was performed visually and *a posteriori* on the output SST product, and considering strips as drop or rise of SST (~ 0.3 °C or more), over few pixels, with an unrealistic rectilinear shape crossing the whole image (Fig. A4). After these quality-checks, 160 matchups could be used to calibrate or validate the various SST algorithms (see section 2.5). Specifically, the numbers of matchups were 24 for Takaroa (18 images), 34 for Tatakoto (26 images), 46 for Raroia (13 images), and 56 for Reao (21 images).

2.5 Satellite-derived-SST calculation

The quality-controlled thermal bands (DN_{10} and DN_{11}) were converted to top-of-atmosphere radiance (TOA_{10} and TOA_{11}), then to 'Brightness Temperature' (BT_{10} and BT_{11}) following the procedure described by Twumasi *et al.* (2021) and using the radiometric conversion factors provided by the USGS image metadata files.

The Non-Linear Sea Surface Temperature (NLSST3) algorithm was used to calculate lagoon SST from a linear combination of BT_{10} and BT_{11} (or their difference), and from the MUR-SST product, following equation 1 (Jang & Park, 2019).

$$NLSST3 = a_1 BT_{10} + a_2 T_{MUR-SST}(BT_{10} - BT_{11}) + a_3 \quad \text{(eq. 1)}$$

Another algorithm was also tested, namely the Multi-Channel Sea Surface Temperature (MCSST1) algorithm (Jang & Park, 2019), but the NLSST3 algorithm was ultimately chosen as it provided better results.

Half of the matchups were used for algorithm calibration and half for validation. In order to calibrate an algorithm which has similar performance over a wide range of temperature, we sorted the matchups by date and sampled data for the calibration and validation sets alternatively, following Kizu and Sakaida (1996). Coefficients a_1, a_2 and a_3 of eq. 1 were optimized so that NLSST3 reflected best the temperature recorded by *in situ* sensors in the calibration dataset of matchups. For this, the Root-Mean-Square-Error (RMSE) was minimized using the Python Scipy library and the Nelder-Mead optimizer (Luersen & Le Riche, 2004; see Fig. A1 for a sensitivity analysis of results according to the optimizer used), and considering a panel of initial values randomly set between 0.001 and 5 (1000 iterations). Optimization was performed individually for each atoll, and for all atolls pooled together. RMSE and bias associated to each simulation were then calculated, using the validation dataset of matchups only.

3. Results

3.1. Spatial variability of temperature from in situ *sensors*

Pairwise differences (absolute value) in hourly-averaged temperature recorded by sensors were slightly higher for Takaroa (0.26°C in mean over all pairwise data available) and Tatakoto (0.25°C) than for Reao (0.17°C) and Raroia (0.19°C; Table 2). Within each lagoon, differences occurred from one site to another.

For Raroia, mean and maximal hourly-mean-temperature difference (in absolute value) between stations were 0.19°C and 1.79°C respectively. *In situ* temperatures were structured in space with gradually increasing temperatures from the north (station RAR4) to the south-western (station RAR6) part of the lagoon. For 42.9% of records, this positive gradient in temperature along the North-eastward/South-westward axis was present with more than 0.1°C difference in hourly-mean-temperature between sensors. This spatial structuration in the North-eastward/South-westward axis occurred more frequently during the warm season (63.1% of records) than during the cool season (25.0% of records; Fig. 2A). By contrast, a negative gradient along this North-eastward/South-westward axis was almost never recorded (0.5% of records). In the lagoon width axis, a positive gradient in temperature (i.e., higher temperature at RAR7 than RAR6 than RAR8) was predominant (46.0% of records), with more occurrences during the warm season (Fig. 2E).

At Takaroa, the sensor deployed in the enclosed and shallow basin located in the southern part of the lagoon (TAK3) usually recorded higher temperature than other sensors (+0.16°C and +0.08°C higher for TAK3 than TAK1 and TAK2 respectively, on average across the measurement period). However, TAK3 was colder during a couple of weeks from May to

August in the cool season. Temperature at TAK3 was higher than at TAK1 with more than 0.1°C difference in hourly-mean-temperature for 59.5% of the records, with stronger occurrence during the warm season (Fig. 2B). Sensor located at TAK2 at proximity of the atoll pass usually recorded temperature higher than TAK1 during the cool season (56.6% of records for which difference was higher than 0.1°C), but the opposite was found during the warm season (61.5% of record; Fig. 2G).

At Reao, temperature recorded by the sensors located on lagoon patch reefs in the northern basin were more variable than in the southern, wide and deeper, basin. Notably, mean difference in hourly-mean-temperature of +0.09°C were recorded between REA10 and REA4 during the warm season, and mean difference of -0.09°C was recorded between these two sensors during the cool season. On the basis of lagoon patch reef sensors REA2, REA9 and REA5, a gradient in temperature along the lagoon length axis was more often negative (i.e., higher temperature at REA2 than at REA9 than at REA5) than positive during the warm season (25.8% *versus* 5.9% of records, respectively), while the reverse was true during the cool season (5.3% *versus* 15.2% of records, respectively; Fig. 2C). Along the lagoon width axis, higher temperature at REA10 than at REA11 with more than 0.1°C difference recorded was found for 49.8% of records (Fig. 2F). In comparison to sensors located on lagoon patch reefs, sensors located on the inner reef flat (REA7), on the wide sandy and shallow terrace located in the eastern part of the lagoon (REA6), and on the inner reef slope (REA8) displayed higher temperature than other sensors when the sun was at zenith, and lower temperature than other sensors at night.

At Tatakoto, the sensor deployed in the enclosed and shallow basin located at the eastern extremity of the lagoon (TAT2) recorded higher temperature than the other sensors (i.e., +0.12 and +0.23 °C higher for TAT2 than TAT1 and TAT3 respectively, on average across the measurement period). On the basis of these three sensors, a negative gradient in temperature was recorded along the lagoon length axis (i.e., higher temperature at TAT2 than at TAT3 than at TAT1) for 18.7% of records, with more occurrences during days than night, independently of season (Fig. 2D).

Temperature differences between sensors were usually higher in the afternoon at Tatakoto (Fig. A2 A). A similar trend was observed at Takaroa, although the daily cycle was less pronounced than Tatakoto (Fig. A2 B). At Reao and Raroia, differences between sensors were the highest in the early afternoon and just before sunrise (Fig. A2 C&D). Episodically, significant differences between some sensors were recorded during several days (night included) to several weeks (Fig. 3). This includes a November 2013 event in both Tatakoto and Takaroa (Fig. 3A and 3B), a November 2018 event at Raroia (Fig. 3C), and a November 2022 event at Reao (Fig. 3D). During these periods of stronger horizontal structuration, the maximum temperature differences recorded between sensors reached 1.36°C, 1.80°C, 1.53°C and 2.4°C for Tatakoto, Takaroa, Raroia, and Reao, respectively.

Because of the L8 satellite overpass hours (09:07 AM for Reao; 09:15 AM for Tatakoto; 09:31 AM for Raroia; 09:45 AM for Takaroa; local time) and long revisit time between consecutive images (16 days minimum), differences in temperature between sensors at time of satellite

overpasses were lower than recorded at other dates and times (Table 2). Considering only the matchup data, the maximum temperature differences recorded between *in situ* sensors were 0.55°C, 1.48°C, 0.88°C, and 0.95°C, for Tatakoto, Takaroa, Raroia, and Reao, respectively.

3.2. Agreement between L8-derived and in situ *temperature*

Best correspondences (lower bias and RMSE) were obtained when optimization was performed atoll by atoll (average bias = -0.26°C; RMSE = 0.55°C) instead of for all atolls together (average bias = -0.30°C; RMSE = 0.60°C; Fig. 4; Table 3). In the best scenario (i.e., atoll-by-atoll calibration), 70.0% of bias values (in absolute values) were below 0.5°C and 92.5% were below 1.0°C. When optimized atoll-by-atoll, significant differences between atolls in algorithm performance were noted, with lowest bias and RMSE for Raroia (average bias = -0.01°C; RMSE = 0.32°C). Highest bias and RMSE were obtained for Takaroa (average bias = -0.60°C; RMSE = 0.79°C), i.e. the lagoon for which the number of matchups available was the lowest.

The maximum temperature difference between stations, estimated by satellite-derived SST, was higher for Reao (1.92°C), while it reached 1.63°C, 0.90°C and 0.68°C for Tatakoto, Takaroa and Raroia respectively (Table 2).

During specific events of high spatial structuration of temperature (e.g., in November 2013 at Takaroa and Tatakoto, November 2018 at Raroia), L8-derived SST did not adequately reproduce the observed differences. Notable differences involved stations at proximity of inner reef slopes, with a 1.16°C overestimation of temperature by L8 at TAT3 on 24th November 2013

(Fig. 3A), a 0.59°C overestimation at TAK1 on 27th November 2013 (Fig. 3B), and a 0.56°C overestimation at RAR8 on 27th November 2018 (Fig. 3C). However, despite these localized problems, L8-derived SST reproduced well the spatial trends recorded by *in situ* sensors. Indeed, in Raroia, the gradual increase from RAR4 to RAR6 which dominates during the warm season (Fig. 2A) was captured by L8 (Fig. 3C and Fig. 5C). Importantly, L8 also captured the thermal footprint of Raroia's reef pass inside the lagoon (Fig. 5C), which could not be captured by the five *in situ* sensors. At Takaroa, L8-derived SST adequately estimated higher temperature in the southern enclosed and shallow basin (Fig. 5A), which is the dominant pattern in the warm season according to *in situ* sensors (Fig. 2B). During the cool season, L8 also captured higher temperature of water around the reef pass (Fig. 5B) in agreement with *in situ* records. Interestingly for this period when ocean water is warmer than lagoon water, L8 also captured warmer water at proximity of *hoa*, and colder water in the north-eastern end of the lagoon where the atoll rim is entirely closed (Fig. 5B). Similarly at Tatakoto, lower SST was found in the south part of the lagoon at proximity of *hoa* during the warm season (Fig. 5E), and *vice versa* during the cool season (Fig. 5F). This gradient in the lagoon width-axis could not be captured by the three *in situ* sensors, whose locality of deployment only allowed the assessment of trends in the lagoon length-axis. Finally at Reao, the negative temperature gradient in the lagoon length axis (i.e., higher temperature in the northern basin than in the middle than in the southern basin), occurring more frequently during the warm season (Fig. 2C), was captured by L8 (Fig. 5G and 5H). Along the lagoon width-axis, the two types of gradients (either positive

or negative; Fig. 2F) could also be captured by L8 (Fig. 5G and 5H). The spatial extrapolation provided by L8 further highlighted lower temperature at proximity of *hoa* when gradient was negative (Fig. 5G), and *vice versa* when gradient was positive (Fig. 5H).

4. Discussion

4.1.Validity and interest of SST algorithms to characterize atoll lagoons

In this study, we demonstrate that the specificities of atoll lagoons do not prevent using L8 imagery for SST retrievals. Indeed, the quality of the relationship between satellite derived SST and *in situ* temperature were satisfying, and RMSE were of the same order of magnitude as in other L8 studies performed elsewhere in the world (Susilo *et al.*, 2019; Jang and Park, 2019; Baughman and Conaway, 2021; Bradtke, 2021). Lower RMSE was found in Indonesia (Syariz *et al.*, 2015), but for a study that focused on a single image. Here, Raroia provided the best relationship and Takaroa the poorest. This may be explained by the fact that Raroia was instrumented with five sensors during a short period of time (46 matchups concentrated on 13 satellite images) whereas Takaroa was instrumented with three sensors during a longer period of time (24 matchups dispersed on 18 satellite images). Thus, the algorithm performances seem dependant on the number of matchups available relative to the number of L8 images used.

The range of temperature inside lagoons is relatively narrow, which may limit the interest of a systematic operationalization of SST algorithms. Indeed, this range was of the same order of magnitude as the RMSE achieved with SST algorithms, except during specific events of high

horizontal structuration. It is worth pointing out that L8-derived SST only partially captured the range of variability that could be measured in the field (Table 2). This can be explained by first, the satellite's time of overpass (between 09:07 AM and 09:45 AM) that miss the time of day when SST differences were the highest. Second, the revisit time of L8 did not allow capturing the events during which temperature spatial gradients were the most pronounced. L8 derived SST nevertheless succeeded in capturing the main gradients inside lagoons, and highlighted spatial patterns that went unnoticed by *in situ* sensors and the MUR SST product, like the incoming jet of the Raroia pass or the lowest temperature in the Northeastern end of Takaroa's lagoon during the cool season (Fig. 5; Fig. A6).

Another important specificity of atoll lagoons are the differences in temperature that can be encountered over small distances due to geomorphological limits, and notably between deeper lagoons and shallow reef flats (Grimaldi *et al.*, 2023; McCabe *et al.*, 2010). Differences between L8 derived SST and *in situ* temperature were the highest for the stations at proximity of inner slopes (e.g., station TAT3, TAK1, RAR8 in Fig. 3). Indeed, near the lagoon slope L8 pixels may include part of the signal emitted by warmer water coming from the reef flats, while *in situ* sensors did not.

Here, we also showed that a L8-based temperature study can characterize well the lagoon-ocean differences. Van Wynsberge *et al.*, (2017; 2020) have quantified with global SST products and *in situ* data how the lagoon is warmer than the ocean in the warm season and cooler in the cool season. These patterns are also detectable with L8 (see Fig. A4), although we could not here

compare with *in situ* sensors located outside the lagoon. These patterns could not be captured by MUR SST for the three smallest lagoons studied here (i.e., Tatakoto, Reao, and Takaroa ; Fig. A6). Although the characterization of the differences between lagoon and ocean temperatures was outside the primary objective of this study, this finding supports the validity of using L8 thermal products to study the atoll lagoons environment.

4.2.Potential improvements for further optimisation of SST algorithms

First, many images in the L8 archive were affected by clouds, which strongly limited the applicability of SST algorithms. Cloud identification and masking is mandatory for SST retrievals, and while cloud filters do exist and can be applied (Zhu and Woodcock, 2012 ; Foga *et al.*, 2017; Chai *et al.*, 2019), they are known to be of insufficient efficacy for accurate SST retrievals, notably near oceanic thermal fronts, near cloud edges, or when hard-to-detect cirrus or stratus clouds are present (Minnett *et al.*, 2019 ; Skakun *et al.*, 2022). Improving cloud masking in SST product, especially in coastal areas, is a priority identified in O'Carroll *et al.* (2019). Here, we performed a manual check to avoid any additional bias, and similar approach could be recommended elsewhere. Specifically developing a cloud masking analytical procedure was however beyond the scope of the present study.

Second, inherent image stripping also reduced in our case the relevance of using L8 images to infer SST. While strips were of minor concern for algorithm calibration (very few strips affected pixels where *in situ* loggers were located), they definitively affected the map product (Fig. 5). Despite the new relative (detector-to-detector) gains included in the level 1 collection 2

processing to reduce along-track striping, these artefacts still affected the set of recent images used in our study. Although not implemented here, methods for image destripping have been recently proposed in the literature (Stumpf *et al.*, 2018; Liu *et al.*, 2020), which could be considered in the near future. Notably, processing level 1 collection 2 with the Thermal Atmospheric Correction Tool (TACT; Vanhellemont, 2020), an open source processor for deriving surface temperature from Landsat sensors based on the libRadtran radiative transfer code (Emde *et al.*, 2016), also allow stripping removal, provided that various atmospheric profiles are available as inputs (Vanhellemont *et al.*, 2022). Beyond the stripping issue, the use of atmospheric corrections performed locally could limit some of the accuracy limitations pointed out here (Zhang *et al.*, 1999).

Third, further improvements in SST algorithm optimisation should address the effects of wind speed and possible bias due to the depth of *in situ* sensors used for algorithm calibration. Indeed, low wind speed leads to vertical water stratification in atolls (Dumas *et al.*, 2012), and to a higher difference between the temperature of the skin layer measured by the satellite and the temperature recorded by deeper sensors. In our study sites, however, vertical temperature stratification between 1 m and 4 m depth remained limited at the hour of L8 overpass (i.e., between 09:07 AM and 09:45 AM depending on atolls), except punctually during very low-wind days (Fig. A8). As a result, the depth of the sensors used for algorithm calibration was not correlated with L8 SST accuracy (Pearson correlation = 0.035, $p = 0.756$), but the absolute value of bias was significantly and negatively correlated with wind speed (Pearson correlation

coefficient of -0.240, $p < 0.05$), with lower wind speed associated with higher bias (Fig. A5). In the light of some authors that found better results when optimizing parameters individually for each month (e.g., Shenoi, 1999; on the basis of NOAA/NESDIS satellite), structuring the calibration process by type of wind conditions may be worth exploring, but will reduce the number of observations available for calibration. Conversely, calibrating SST algorithms using only the shallowest *in situ* sensors would certainly reduce RMSE, but such an approach is not strictly mandatory for fisheries and aquaculture applications, for which estimating bulk temperature (i.e. a temperature more representative of the environment experienced by organisms) is actually of greater interest than estimating skin-temperature.

Finally, some authors working with VIIRS and MODIS images have shown that column water vapor content in the atmosphere and satellite view zenith angle have a strong impact on SST, so it is advisable to set coefficients a_1, a_2, and a_3 for SST calculation (see eq. 1) specifically for each latitude (Petrenko *et al.*, 2014), or to explicitly take zenith angle into account in SST algorithms (Kilpatrick *et al.*, 2015). Here, the effect of satellite zenith angle has been implicitly considered in the atoll-by-atoll scenario, since coefficients have been set individually for each lagoon. Taking explicitly zenith angle into account in SST equations is, by contrast, not necessary for the purpose of generating maps of SST inside instrumented lagoons with L8. Indeed, the L8 scene size is 185 km (cross track) by 180 km (along-track), and satellite zenith angle of L8 is always 0 at the centre of a scene. Thus, for a given location, the satellite zenith angle does not change between images (i.e., across time). From one side of a scene to the other

(east-west direction), differences in satellite zenith angle remain below 9 degrees, which is lower than other satellites (AVHRR, MODIS, and Sentinel) and has little effect on SST estimates (Jang and Park, 2019). Considering the small length of atoll lagoons studied here (from 11 km for Tatakoto to 38 km for Raroia), difference in zenith angle inside a given lagoon is negligible, and considering this factor is not necessary when the purpose of the study is mapping SST inside instrumented lagoons.

4.3. Relevance of L8 derived SST for other atoll lagoons

The four atoll lagoons processed in this study are diverse in their sizes, morphologies and degree of aperture to the ocean (from semi-closed to semi-open). The satisfying performance of L8 SST algorithms obtained for all four atolls regardless of their characteristics gives us confidence in the reliability of transposing the method to other instrumented atolls. For lagoons that are not instrumented with temperature sensors, the optimization performed all atolls confounded may provide a good first guess and model, until local (lagoon specific) data become available. Although algorithms were less accurate when calibrated with all atoll data instead of atoll by atoll, the degradation was moderate, going from bias = -0.26°C (atoll by atoll) to -0.30°C (all atolls), and with an increase of RMSE from 0.55°C (atoll by atoll) to 0.60°C (all atoll). These results are quite encouraging to attempt a universal relationship between temperature and L8 infrared bands, valid first for all Tuamotu atolls.

4.4. Applications of L8 SST retrievals for Tuamotu atolls

The SST map products inferred from L8 imagery can assist research and management in Tuamotu atolls in various ways. First, it can help depict daily horizontal thermal gradients and fronts occurring inside atoll lagoons and thus provide useful information for the validation of spatial patterns that could come from hydrodynamic models as in Dumas *et al.*, (2012). This knowledge cannot be acquired using a necessary low number of deployable *in situ* loggers (Kowalewska-Kalkowska and Kowalewski, 2019). If SST maps depicting a variety of atmospheric and oceanic conditions are available, they could help understanding lagoon thermal variability, as well as relevant hydrodynamic processes.

Second, SST maps from L8 could help designing sampling strategy for new *in situ* collection of any temperature or other temperature-dependant variable (e.g., growth of biological organisms), by identifying areas inside lagoon that may be thermally contrasted. Indeed, the dominant gradients in temperature that affected the studied lagoons could be adequately pictured here and could be used to guide sampling.

Third, L8 derived SST can provide a source of information on temperature at lagoon scale, when no other information is available (i.e., no *in situ* sensors, and no reliable estimates from Global SST products). Owing to the time period covered by L8 mission (from 2013 to present), and its revisit time, the L8 SST product could be useful to calculate a first climatology (e.g.,

monthly mean temperature over ten year) relevant for the lagoons if there are enough data. A climatological baseline is a prerequisite to calculate thermal stress indexes for marine resources, but is currently lacking for small lagoons where global SST products are not reliable (Van Wynsberge *et al.*, 2017).

Finally, SST map products inferred from L8 imagery may inform spatial planning studies, as systematic conservation planning tools evolve toward scenarios that better take temperature data and climate change into account (Petrosillo *et al.*, 2023). However, spatial planning studies require spatially exhaustive data (i.e., no spatial gaps in data; Moilanen *et al.*, 2009), which is a limitation in the case of L8 derived SST owing to the low frequency of revisit time and the very few numbers of cloud-free (and strip-free) images. Other satellites may be valid sources of 11 µm and 12 µm infrared bands with higher frequency revisit time than L8. This is the case of the recently launched Landsat-9 satellite, which, combined with L8, could provide images at 8 days' frequency. A cross-calibration analysis between L8 and Landsat-9 sensors showed excellent results between the two products (Gross *et al.*, 2023), which suggests that the work performed here will remain of value and generalizable with Landsat 9 images. The ECOsystem Spaceborne Thermal Radiometer Experiment on Space Station (ECOSTRESS) mission on the International Space Station since June 2018, the upcoming Franco-Indian CNES/ISRO TRISHNA mission foreseen in 2026, and the ESA High Priority Copernicus Land Surface Temperature Monitoring (LSTM) mission foreseen in 2028 are now available or on their way,

and will provide better radiometric performances, higher spatial resolution and temporal sampling and increase the value and operational capacity of this source of observation.

5. Conclusion

We demonstrated that the range of temperature inside atoll lagoons is of the same order of magnitude as the RMSE associated with SST algorithms, but nevertheless confirm the interest of a systematic operationalization of SST algorithms for these water bodies. Notably, and despite that L8 SST could only partially capture the range of variability that could be encountered in the field, it could characterize spatial gradients and fronts more comprehensively than with few *in situ* sensors. Indeed, L8 derived SST succeeded in capturing the main gradients inside lagoons, and highlighted spatial patterns that went unnoticed by *in situ* sensors and the MUR SST product. The set of parameter values provided in this study should be relevant for most of the 598 world's atolls, but we recommend using local estimates of SST parameters whenever possible.

6. Acknowledgements

This work was supported by the Agence National de la Recherche [ANR-21-CE32-0011-01 GAIA and ANR-16-CE32-0004 MANA]; Direction des Ressources Marines of French Polynesia [OTI project Contrat de Projet France-French Polynesia, Program 123, Action 2, 2015–2020]; the Grand Observatoire du Pacifique Sud [CITADEL project]; MALIS 1 and

MALIS 2 oceanographic cruises in Raroia Atoll on board the RV Alis (https://doi.org/10.17600/18000582); and by the CNES TOSCA TRISHNA Coastal and Inland Waters project. We also thanks M. Pahuatini, M. Teara, L. Poltavtseef, T. Richmond, V. Teaniniuraitemoana, C. Monaco, M. Célariès, P. Maere, A. Rata, G. Haumani, R/V Alis crew as well as T. Trophime, V. Liao, J. Campanozzi-Tarahu, F. Tertre, C. Germain, J. Aucan, D. Varillon, J. Butscher, and B. Bourgeois for their help during field trips dedicated to logger maintenance. Finally, we thank two anonymous reviewers, who made constructive comments that improved significantly this paper.

7. References

Andréfouët, S., 2018. MALIS 1&2 cruise, RV Alis. https://doi.org/10.17600/18000582.

Andréfouët, S., Van Wynsberge, S., Kabbadj, L., Wabnitz, C.C.C., Menkes, C., Tamata, T., Pahuatini, M., Tetairekie, I., Teaka, I., Scha, T.A., Teaka, T., Remoissenet, G., 2018. Adaptive management for the sustainable exploitation of lagoon resources in remote islands: lessons from a massive El Niño-induced giant clam bleaching event in the Tuamotu atolls (French Polynesia). *Environmental Conservation* 45(1), 30–40. https://doi.org/10.1017/S0376892917000212.

Andréfouët, S., Genthon, P., Pelletier, B., Le Gendre, R., Friot, C., Smith, R., & Liao, V., 2020. The lagoon geomorphology of pearl farming atolls in the Central Pacific Ocean revisited using

detailed bathymetry data. *Marine Pollution Bulletin* 160, 111580. https://doi.org/10.1016/j.marpolbul.2020.111580.

Andréfouët, S., Bruyère, O., Liao, V., & Le Gendre, R., 2023. Hydrodynamical impact of the July 2022 'Code Red'distant mega-swell on Apataki Atoll, Tuamotu Archipelago. *Global and Planetary Change*, *228*, 104194. https://doi.org/10.1016/j.gloplacha.2023.104194.

Andréfouët, S., & Paul, M., 2023. Atolls of the world: A reappraisal from an optical remote sensing and global mapping perspective. *Marine Pollution Bulletin* 194, 115400. https://doi.org/10.1016/j.marpolbul.2023.115400.

Aucan, J., Desclaux, T., Le Gendre, R., Liao, V., Andréfouët, S., 2021. Tide and wave driven flow across the rim reef of the atoll of Raroia (Tuamotu, French Polynesia). *Marine Pollution Bulletin* 171, 112718. https://doi.org/10.1016/j.marpolbul.2021.112718.

Barnes, M.L., Miura, T., Giambelluca, T.W., 2016. An Assessment of Diurnal and Seasonal Cloud Cover Changes over the Hawaiian Islands Using Terra and Aqua MODIS. *Journal of Climate* 29(1), 77-90. https://doi.org/10.1175/JCLI-D-15-0088.1.

Baughman, C.A., Conaway, J.S., 2021. Comparison of Historical Water Temperature Measurements with Landsat Analysis Ready Data Provisional Surface Temperature Estimates for the Yukon River in Alaska. *Remote Sensing* 13, 2394. https://doi.org/10.3390/rs13122394.

Beggs, H., Zhong, A., Warren, G., Alves, O., Brassington, G., and Pugh, T., 2011. RAMSSA - an operational, high-resolution, regional Australian multi-sensor sea surface temperature

analysis over the Australian region. *Australian Meteorological and Oceanographical Journal* 61, 1–22. https://doi:10.22499/2.6101.001.

Belkin, I.M., 2021. Remote sensing of ocean fronts in marine ecology and fisheries. *Remote Sensing* 13(5), 883. https://doi.org/10.3390/rs13050883.

Bell, J.D., Johnson, J.E., Hobday, A.J. (Eds.), 2011. *Vulnerability of tropical Pacific fisheries and aquaculture to climate change*. Pacific Community, Auckland, New Zealand, 927 pp.

Bradtke, K., 2021. Landsat 8 data as a source of high resolution sea surface temperature maps in the Baltic sea. *Remote Sensing* 13(22). https://doi.org/10.3390/rs13224619.

Bruyère, O., Le Gendre, R., Chauveau, M., Bourgeois, B., Varillon, D., Butscher, J., Trophime, T., Follin, Y., Aucan, J., Liao, V., Andréfouët, S., 2023a. Lagoon hydrodynamics of pearl farming atolls: the case of Raroia, Takapoto, Apataki and Takaroa (French Polynesia). *Earth System Science Data* 15, 5553–5573. https://doi.org/10.5194/essd-15-5553-2023.

Bruyère, O., Chauveau, M., Le Gendre, R., Liao, V., Andréfouët, S., 2023b. Larval dispersal of pearl oysters Pinctada margaritifera in the Gambier Islands (French Polynesia) and exploring options for adult restocking using in situ data and numerical modelling. *Marine Pollution Bulletin* 192, 115059. https://doi.org/10.1016/j.marpolbul.2023.115059.

Bruyère, O., Le Gendre, R., Liao, V., Andréfouët, S., 2024. Lagoon hydrodynamics of pearl farming islands: the case of Gambier (French Polynesia). *Earth System Science Data Discussions* 16, 667-679. https://doi.org/10.5194/essd-16-667-2024.

Canavesio, R., 2019. Distant swells and their impacts on atolls and tropical coastlines. The example of submersions produced by lagoon water filling and flushing currents in French Polynesia during 1996 and 2011 mega swells. *Global and Planetary Change* 177, 116–126. https://doi.org/10.1016/j.gloplacha.2019.03.018.

Chai, D., Newsam, S., Zhang, H.K., Qiu, Y., Huang, J., 2019. Cloud and cloud shadow detection in Landsat imagery based on deep convolutional neural networks. *Remote Sensing of Environment* 225, 307–316. https://doi.org/10.1016/j.rse.2019.03.007.

Chin, T.M., Vazquez-Cuervo, J., Armstrong, E.M., 2017. *A multi-scale high-resolution analysis of global sea surface temperature* 200, 154-169. https://doi.org/10.1016/j.rse.2017.07.029.

Dash P., Ignatov, A., Martin, M., Donlon, C., Brasnett, B., Reynolds, R.W., Banzon, V., Beggs, H., Cayula, J.F., Chao, Y., Grumbine, R., Maturi, E., Harris, A., Mittaz, J., Snapper, J., Chin, T.M., Vazquez-Cuervo, J., Armstrong, E.M., Gentemann, C., Cummings, J., Piollé, J.F., Autret, E., Roberts-Jones, J., Ishizaki, S., Hoyer, J.L., Poulter, D., 2012. Group for High Resolution Sea Surface Temperature (GHRSST) analysis fields inter-comparisons-Part 2: Near real time web-based level 4 SST Quality Monitor (L4-SQUAM). *Deep Sea Research Part II: Tropical Studies in Oceanography* 77-80, 31-43. http://dx.doi.org/10.1016/j.dsr2.2012.04.002.

Dumas, F., Le Gendre, R., Thomas, Y., Andréfouët, S., 2012. Tidal flushing and wind driven circulation of Ahe atoll lagoon (Tuamotu Archipelago, French Polynesia) from *in situ*

observations and numerical modelling. *Marine Pollution Bulletin* 65(10-12), 425-440. https://doi.org/10.1016/j.marpolbul.2012.05.041.

Dutheil, C., Andréfouët, S., Jullien, S., Le Gendre, R., Aucan, J., Menkes, C., 2020. Characterization of South Central Pacific Ocean wind regimes in present and future climate for pearl farming application 160, 111584. https://doi.org/10.1016/j.marpolbul.2020.111584.

Eladawy, A., Nakamura, T., Shaltout, M., Mohammed, A., Nadaoka, K., Fox, M. D., Osman, E.O., 2022. Appraisal of coral bleaching thresholds and thermal projections for the northern Red Sea refugia. *Frontiers in Marine Science* 9, 938454. https://doi.org/10.3389/fmars.2022.938454.

Emde, C., Buras-Schnell, R., Kylling, A., Mayer, B., Gasteiger, J., Hamann, U., Kylling, J., Richter, B., Pause, C., Dowling, T., Bugliaro, L., 2016. The libRadtran software package for radiative transfer calculations (version 2.0. 1). *Geoscientific Model Development* 9(5), 1647–1672. https://doi.org/10.5194/gmd-9-1647-2016.

Foga, S., Scaramuzza, P.L., Guo, S., Zhu, Z., Dilley, R.D., Beckmann, T., Schmidt, G.L., Dwyer, J.L., Hughes, M.J., Laue, B., 2017. Cloud detection algorithm comparison and validation for operational Landsat data products. *Remote Sensing of Environment* 194, 379-390, ISSN 0034-4257. https://doi.org/10.1016/j.rse.2017.03.026.

Gorelick, N., Hancher, M., Dixon, M., Ilyushchenko, S., Thau, D., Moore, R., 2017. Google Earth Engine: Planetary-scale geospatial analysis for everyone. *Remote Sensing of Environment* 202, 18-27. https://doi.org/10.1016/j.rse.2017.06.031.

Grimaldi, C.M., Lowe, R.J., Benthuysen, J.A., Cuttler, M.V.W., Green, R.H.J., Gilmour P., 2023. Hydrodynamic and atmospheric drivers create distinct thermal environments within a coral reef atoll. *Coral Reefs* 42, 693-706. https://doi.org/10.1007/s00338-023-02371-x.

Gross, G., Helder, D., Leigh, L., 2023. Extended Cross-Calibration Analysis Using Data from the Landsat 8 and 9 Underfly Event. *Remote Sensing* 15(7), 1788. https://doi.org/10.3390/rs15071788.

Heron, S.F., Liu, G., Eakin, C.M., Skirving, W.J., Muller-Karger, F.E., Vega-Rodriguez, M., De la Cour, J.L., Burgess, T.F.R., Strong, A.E., Geiger, E.F., Guild, L.S., Lynds, S., 2015. Climatology Development of NOAA Coral Reef Watch's 5-km Product Suite. Technical Report NESDIS 145. National Oceanic and Atmospheric Administration's National Environmental Satellite, Data, and Information Service, Coral Reef Watch, College Park, MD. 21p. https://doi.org/10.7289/V59C6VBS.

Jang, J.C., Park, K.A., 2019. High-resolution sea surface temperature retrieval from Landsat 8 OLI/TIRS data at coastal regions. *Remote Sensing* 11(22), 2687. https://doi.org/10.3390/rs11222687.

Kilpatrick, K.A., Podestá, G., Walsh, S., Williams, E., Halliwell, V., Szczodrak, M., Brown, O.B., Minnett, P.J., Evans, R., 2015. A decade of sea surface temperature from MODIS. *Remote Sensing of Environment* 165, 27–41. https://doi.org/10.1016/j.rse.2015.04.023.

Kizu, S., Sakaida, F., 1996. A new set of MCSST equations for NOAA-9/AVHRR. *Journal of Oceanography* 52, 235-249. https://doi.org/10.1007/BF02235672.

Klemas, V., 2013. Fisheries applications of remote sensing: An overview. *Fisheries Research* 148, 124-136. https://doi.org/10.1016/j.fishres.2012.02.027.

Kowalewska-Kalkowska, H., Kowalewski, M., 2019. Combining Satellite Imagery and Numerical Modelling to Study the Occurrence of Warm Upwellings in the Southern Baltic Sea in Winter. *Remote Sensing* 11(24), https://doi.org/10.3390/rs11242982.

Lee, ST., Cho, YK., Kim, D.J., 2022. Immense variability in the sea surface temperature near macro tidal flat revealed by high-resolution satellite data (Landsat 8). *Scientific Reports* 12, 248. https://doi.org/10.1038/s41598-021-04465-4.

Liu, M., Yin, X., Xu, Q., Chen, Y., Wang, B., 2020. Monitoring of fine-scale warm drain-off water from nuclear power stations in the daya bay based on landsat 8 data. *Remote Sensing* 12(4), 627. https://doi.org/10.3390/rs12040627

Luersen, M.A., Le Riche, R., 2004. Globalized Nelder–Mead method for engineering optimization. *Computers & structures* 82(23-26), 2251-2260. https://doi.org/10.1016/j.compstruc.2004.03.072.

McCabe, R.M., Estrade, P., Middleton, J.H., Melville, W.K., Roughan, M., Lenain, L., 2010. Temperature variability in a shallow, tidally isolated coral reef lagoon. *Journal of geophysical research* 115(C12), C12011. https://doi.org/10.1029/2009JC006023.

Melet, A., Teatini, P., Le Cozannet, G., Jamet, C., Conversi, A., Benveniste, J., & Almar, R., 2020. Earth observations for monitoring marine coastal hazards and their drivers. *Surveys in Geophysics* 41, 1489-1534. https://doi.org/10.1007/s10712-020-09594-5.

Minnett, P.J., Alvera-Azcárate, A., Chin, T.M., Corlett, G.K., Gentemann, C.L., Karagali, I., Li, X., Marsouin, A., Marullo, S., Maturi, E., Santoleri, R., Saux Picart, S., Steele, M., Vazquez-Cuervo, J., 2019. Half a century of satellite remote sensing of sea-surface temperature. *Remote Sensing of Environment* 233, 111366. https://doi.org/10.1016/j.rse.2019.111366.

Moilanen, A., Wilson, K., Possingham, H. (Eds.), 2009. Spatial Conservation Prioritization: Quantitative Methods and Computational Tools. Oxford University Press, Oxford; New York.

Monaco, C.J., Sangare, N., Le Moullac, G., Basset, C., Belliard, C., Mizuno, K., Smith, D.L., Lo-Yat, A., 2021. Dynamic Energy Budget model suggests feeding constraints and physiological stress in black-lip pearl oysters, 5 years post mass-mortality event. *Marine Pollution Bulletin* 167, 112329. https://doi.org/10.1016/j.marpolbul.2021.112329.

Mondejar, J.P., Tongco, A.F., 2019. Near infrared band of Landsat 8 as water index: a case study around Cordova and Lapu-Lapu City, Cebu, Philippines. *Sustainable Environment Research* 29, 16. https://doi.org/10.1186/s42834-019-0016-5.

O'carroll, A.G., Armstrong, E.M., Beggs, H.M., Bouali, M., Casey, K.S., Corlett, G.K., Dash, P., Donlon, C.J., Gentemann, C.L., Hoyer, J.L., Ignatov, A., Kabobah, K., Kachi, M., Kurihara, Y., Karagali, I., Maturi, E., Merchant, C.J., Marullo, S., Minnett, P.J., Pennybacker, M., Ramakrishnan, B., Ramsankaran, R., Santoleri, R., Sunder, S., Saux Picard, S., Vazquez-Cuervo, J., Wimmer, W., 2019. Observational needs of sea surface temperature. *Frontiers in Marine Science 6*, 420. https://doi.org/10.3389/fmars.2019.00420.

Palmer, S.C., Gernez, P.M., Thomas, Y., Simis, S., Miller, P.I., Glize, P., & Barillé, L., 2020. Remote sensing-driven Pacific oyster (*Crassostrea gigas*) growth modeling to inform offshore aquaculture site selection. *Frontiers in Marine Science 6*, 802. https://doi.org/10.3389/fmars.2019.00802.

Petrenko, B., Ignatov, A., Kihai, Y., Stroup, J., Dash, P., 2014. Evaluation and selection of SST regression algorithms for JPSS VIIRS, JGR Atmospheres 119, 4580–4599. https://doi.org/10.1002/2013JD020637.

Petrosillo, I., Scardia, A.M.S., Ungaro, N., Specchiulli, A., Fanelli, G., Centoducati, G., De Serio, F., Carlucci, R., Valente, D., Barbone, E., Pini, A., Giannuzzi, C.G., Scirocco, T., Lovello, E.M., Deflorio, M., Lillo, A.O., De Padova, D., Papa., L., Goffredo, E., Mancini, M.E., Mossa, M., 2023. Towards sustainable marine spatial planning of aquaculture. *Ecological Indicators* 154, 110542. https://doi.org/10.1016/j.ecolind.2023.110542.

Rodier, M., Longo, S., Henry, K., Ung, A., Lo-Yat, A., Darius, H., Viallon, J., Beker, B., Delesalle, B., Chinain, M., 2019. Diversity and toxic potential of algal bloom-forming species from Takaroa lagoon (Tuamotu, French Polynesia): a field and mesocosm study. *Aquatic Microbial Ecology* 83(1), 15–34. https://doi.org/10.3354/ame01900.

Shenoi, S.C., 1999. On the suitability of global algorithms for the retrieval of SST from the north Indian Ocean using NOAA/AVHRR data. *International Journal of Remote Sensing* 20(1), 11-29. https://doi.org/10.1080/014311699213578.

Skakun, S., Wevers, J., Brockmann, C., Doxani, G., Aleksandrov, M., Batič, M., Frantz, D., Gascon, F., Gómez-Chova, L., Hagolle, O., López-Puigdollers, D., Louis, J., Lubej, M., Mateo-García, G., Osman, J., Peressutti, D., Pflug, B., Puc, J., Richter, R., Roger, J.C., Scaramuzza, P., Vermote, E., Vesel, N., Zupanc, A., Žust, L., 2022. Cloud Mask Intercomparison eXercise (CMIX): An evaluation of cloud masking algorithms for Landsat 8 and Sentinel-2. *Remote Sensing of Environment* 274, 112990, ISSN 0034-4257. https://doi.org/10.1016/j.rse.2022.112990.

Snyder, J., Boss, E., Weatherbee, R., Thomas, A.C., Brady, D., Newell, C., 2017. Oyster Aquaculture Site Selection Using Landsat 8-derived Sea Surface Temperature, Turbidity, and Chlorophyll a. *Frontiers in Marine Science* 4, 190. https://doi.org/10.3389/fmars.2017.00190.

Stumpf, A., Michéa, D., Malet, J.P., 2018. Improved Co-Registration of Sentinel-2 and Landsat-8 Imagery for Earth Surface Motion Measurements. *Remote Sensing* 10(2), 160. https://doi.org/10.3390/rs10020160.

Susilo, E., Hanintyo, R., Wijaya, A., 2019. Retrieving Coastal Sea Surface Temperature from Landsat-8 TIRS For Wangi-Wangi Island, Wakatobi, Southeast Sulawesi, Indonesia. *International Journal of Remote Sensing and Earth Sciences* 16(1), 13-22. http://dx.doi.org/10.30536/j.ijreses.2019.v16.a3044.

Syariz, M., Jaelani, L., Subehi, L., Pamungkas, A., Koenhardono, E., Sulisetyono, A., 2015. Retrieval of sea surface temperature over poteran island water of indonesia with Landsat 8 TIRS image: A preliminary algorithm. ISPRS - *International Archives of the Photogrammetry, Remote Sensing and Spatial Information Sciences* XL-2/W4, 87-90. https://doi.org/10.5194/isprsarchives-XL-2-W4-87-2015.

Thomas, Y., Dumas, F., Andréfouët, S., 2016. Larval connectivity of pearl oyster through biophysical modelling; evidence of food limitation and broodstock effect. *Estuarine, Coastal and Shelf Science* 182, 283-293. https://doi.org/10.1016/j.ecss.2016.03.010.

Trinh, R.C., Fichot, C.G., Gierach, M.M., Holt, B., Malakar, N.K., Hulley, G., Smith, J., 2017. Application of Landsat 8 for Monitoring Impacts of Wastewater Discharge on Coastal Water Quality. *Frontiers in Marine Science* 4, ISSN 2296-7745. https://doi.org/10.3389/fmars.2017.00329.

Twumasi, Y.A., Merem, E.C., Namwamba, J.B., Mwakimi, O.S., Ayala-Silva, T., Frimpong, D.B., Ning, Z.H., Asare-Ansah, A.B., Annan, J.B., Oppong, J., Loh, P.M., Owusu, F., Jeruto, V., Petja, B.M., Okwemba, R., McClendon-Peralta, J., Akinrinwoye, C.O. and Mosby, H.J., 2021. Estimation of Land Surface Temperature from Landsat-8 OLI Thermal Infrared Satellite Data. A Comparative Analysis of Two Cities in Ghana. *Advances in Remote Sensing* 10, 131-149. https://doi.org/10.4236/ars.2021.104009.

Vanhellemont, Q., 2020. Automated water surface temperature retrieval from Landsat 8/TIRS. *Remote Sensing of Environment* 237, 111518. https://doi.org/10.1016/j.rse.2019.111518.

Vanhellemont, Q., Brewin, R.J.W., Bresnahan, P.J., Cyronak, T., 2022. Validation of Landsat 8 high resolution Sea Surface Temperature using surfers. *Estuarine, Coastal and Shelf Science* 265, 107650. https://doi.org/10.1016/j.ecss.2021.107650.

Van Wynsberge, S., Menkes, C., Le Gendre, R., Passfield, T., Andréfouët, S., 2017. Are Sea Surface Temperature satellite measurements reliable proxies of lagoon temperature in the South Pacific? *Estuarine, Coastal and Shelf Science* 199, 117–124. https://doi.org/10.1016/j.ecss.2017.09.033.

Van Wynsberge, S., Le Gendre, R., Sangare, N., Aucan, J., Menkes, C., Liao, V., Andréfouët, S., 2020. Monitoring pearl farming lagoon temperature with global high resolution satellite-derived products: An evaluation using Raroia Atoll, French Polynesia. *Marine Pollution Bulletin* 160, 111576. https://doi.org/10.1016/j.marpolbul.2020.111576.

Varillon, D., Fiat, S., Magron, F., Allenbach, M., Hoibian, T., De Ramon N'Yeurt, A., Ganachaud, A., Aucan, J., Pelletier, B., & Hocdé, R., 2019. *ReefTEMPS : The Pacific Island coastal ocean observation network* [Data set]. SEANOE. https://doi.org/10.17882/55128.

Wabnitz, C.C.C., Remoissenet, G., 2012. Postlarval capture and culture of Tridacna maxima giant clams in French Polynesia. *SPC Fisheries Newsletter* 139, 16-19.

Wang, D., Pan, D., Wei, J.A., Gong, F., Zhu, Q., Chen, P., 2016. Monitoring thermal discharge from a nuclear plant through Landsat 8, *Proc. SPIE 9999, Remote Sensing of the Ocean, Sea Ice, Coastal Waters, and Large Water Regions* 99991E. https://doi.org/10.1117/12.2242253.

Xing, Q., Chen, C.Q., Shi, P., 2006. Method of integrating landsat-5 and landsat-7 data to retrieve sea surface temperature in coastal waters on the basis of local empirical algorithm. *Ocean Science Journal* 41, 97-104. https://doi.org/10.1007/BF03022414.

Zhang, M., Carder, K., Muller-Karger, F.E., Lee, Z., Goldgof, D.B., 1999. Noise Reduction and Atmospheric Correction for Coastal Applications of Landsat Thematic Mapper Imagery. *Remote Sensing of Environment* 70, 167–180. https://doi.org/10.1016/S0034-4257(99)00031-0.

Zhu, Z., Woodcock, C.E., 2012. Object-based cloud and cloud shadow detection in Landsat imagery, *Remote Sensing of Environment* 118, 83-94, ISSN 0034-4257. https://doi.org/10.1016/j.rse.2011.10.028.

Tables

Table 1: Characteristics of *in situ* sensor time series used in this study.

Location	Station	Latitude	Longitude	Sensor Type	Depth (m)	Measurement type	Deployment time period	Measurement frequency	Number of high-quality matchups with L8
Reao	REA1	-18.494014	-136.411855	TWR2050	3.6	T, P	16/12/2016 – 29/06/2017	30’	3
Reao	REA2	-18.483047	-136.424779	SBE56	1.3	T	08/06/2021– 02/06/2023	20’	7
Reao	REA4	-18.565526	-136.333066	SBE56	1.7	T	30/04/2022 – 02/06/2023	30’	4
Reao	REA5	-18.543180	-136.342201	SBE56	1.8	T	30/04/2022 – 02/06/2023	30’	6
Reao	REA6	-18.521482	-136.356377	SBE56	1.3	T	30/04/2022 – 02/06/2023	30’	5
Reao	REA7	-18.513607	-136.390002	SBE56	1.2	T	30/04/2022 – 02/06/2023	30’	8
Reao	REA8	-18.501160	-136.376241	SBE56	1.4	T	30/04/2022 – 02/06/2023	30’	7
Reao	REA9	-18.497568	-136.396765	SBE56	1.4	T	30/04/2022 – 02/06/2023	30’	4
Reao	REA10	-18.481026	-136.442612	SBE56	1.2	T	30/04/2022 – 02/06/2023	30’	9
Reao	REA11	-18.472794	-136.435903	RBR Duet	1.5	T, P	07/05/2022 – 14/04/2023	15’	3
Raroia	RAR4	-15.987153	-142.364223	SBE56	2.1	T	25/05/2018 – 23/03/2019	10’	13
Raroia	RAR5	-16.064706	-142.418871	SBE56	2.0	T	25/05/2018 – 22/03/2019	10’	9

Raroia	RAR6	-16.150752	-142.468992	SBE56	2.5	T	27/05/2018 – 22/03/2019	10’	8
Raroia	RAR7	-16.117779	-142.502806	SBE56	1.8	T	27/05/2018 – 23/03/2019	10’	8
Raroia	RAR8	-16.153191	-142.410957	SBE56	2.4	T	27/05/2018 – 23/03/2019	10’	8
Tatakoto	TAT1	-17.3488	-138.435	SBE56	1.0	T	11/11/2012 - 24/10/2017	30’	16
Tatakoto	TAT2	-17.3334	-138.351	SBE56	2.8	T	11/11/2012 - 15/08/2017	30’	15
Tatakoto	TAT3	-17.3508	-138.41	RBRduo	3.4	T, P	16/11/2012 - 22/10/2014	30’	3
Takaroa	TAK1	-14.5026	-145.01605	SBE56	4.0	T	01/12/2012 - 19/03/2016	30’	10
Takaroa	TAK2	-14.473967	-145.02955	RBRduo	4.0	T, P	30/11/2012 – 04/06/2015	30’	3
Takaroa	TAK3	-14.5076	-145.052367	SBE56	2.0	T	01/12/2012 – 18/01/2016	30’	8
Takaroa	TAK4	-14.45972	-144.95946	NKE Sambat	4.0	T, F	30/01/2019 – 24/02/2021	60’	3

Table 2: Spatial variability of temperature inside atoll lagoons measured by sensors and captured by L8 imagery for the geographic positions of each temperature sensor. Only sensors located in the lagoon *sensu stricto* (but inner slope included) were included (i.e., T7 at Reao located on the reef flat was not considered for computing these statistics). For *in situ* data, statistics were computed on hourly mean temperature data, and "difference" refers to absolute values of differences (subtracting) of pair-wise sensors temperatures. Note that these values are necessarily constrained by sampling scheme inherent to each lagoon.

Lagoon	Data selected for computing statistics	Max temperature difference between sensors (°C)	Mean temperature difference between sensors (°C)	Max temperature difference by satellite (°C)	Mean temperature difference by satellite (°C)
Reao	All *in situ* data	1.67	0.17		
	Match ups only	0.95	0.32	1.92	1.01
Raroia	All *in situ* data	1.79	0.19		
	Match ups only	0.88	0.38	0.68	0.40
Takaroa	All *in situ* data	2.27	0.26		
	Match ups only	1.48	0.54	0.90	0.27
Tatakoto	All *in situ* data	2.31	0.25		
	Match ups only	0.55	0.30	1.63	0.43

Table 3: Coefficients estimated and performance of the fit obtained for the NLSST3 algorithm, when fitted on high quality data only. Results are provided for optimizations performed atoll by atoll and for optimizations performed all atolls confounded. n: number of matchups available (half used for setting coefficients, and half for computing bias and RMSE).

Scale for optimization	Lagoon	n	Coefficient a1	Coefficient a2	Coefficient a3	Bias	RMSE
Atoll by atoll	Reao	56	0.49181	0.06536	6.27719	-0.33	0.54
	Tatakoto	34	0.44197	0.07854	4.85649	-0.24	0.62
	Takaroa	24	0.51607	0.06143	5.41305	-0.60	0.79
	Raroia	46	0.46515	0.06883	6.27148	-0.01	0.32
All atolls confounded	All	160	0.48823	0.0666	5.87312	-0.30	0.60

Figure Legends

Figure 1 : Study site locations. **A)** Locations of the four atolls studied in Tuamotu archipelago, French Polynesia. **B-E)** Satellite view of the four studied sites (L8 images captured on 7/11/2021, 17/01/2016, 07/7/2019, and 27/11/2018 for Reao, Tatakoto, Takaroa, and Raroia respectively) and location of in situ temperature sensors used for SST algorithm optimization. The two nearest stations REA10 and REA11 are 1,15 km apart.

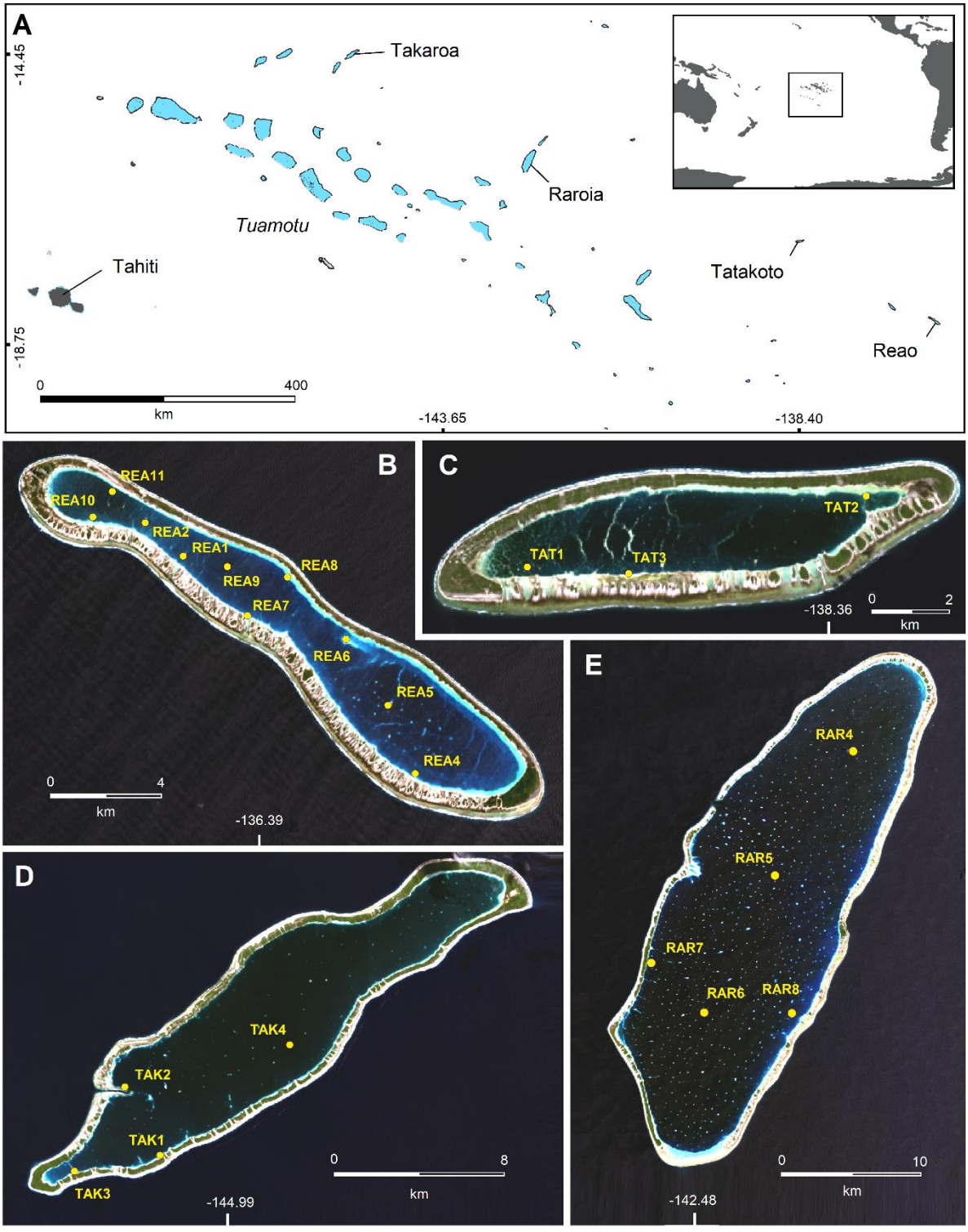
A
-14.45
-18.75
Takaroa
Raroia
Tuamotu
Tahiti
Tatakoto
Reao
0
400
km
-143.65
-138.40
B
REA11
REA10
REA2
REA1
REA8
REA9
REA7
REA6
REA5
REA4
0
4
km
-136.39
C
TAT2
TAT1
TAT3
-138.36
0
2
km
D
TAK4
TAK2
TAK1
TAK3
0
8
km
-144.99
E
RAR4
RAR5
RAR7
RAR6
RAR8
0
10
km
-142.48

Figure 2: Proportion of time for which a gradient in temperature was recorded by sensors along the lagoon length axis, at Raroia **(A)**, Takaroa **(B)**, Reao **(C)**, Tatakoto **(D)**, and along the lagoon width axis, at Raroia **(E)**, Reao **(F)**, and Takaroa **(G)**. In panels A-D, a "positive" gradient refers to an increasing temperature (≥ 0.1°C) recorded between RAR4, RAR5 and RAR6 at Raroia, between TAK1 and TAK3 at Takaroa, between REA2, REA9 and REA5 at Reao, and between TAT2, TAT3 and TAT1 at Tatakoto, and *vice versa* for negative gradients. In panels E-G, A "positive" gradient refers to an increasing temperature (≥ 0.1°C) recorded between RAR8, RAR6 and RAR7 at Raroia, between REA11 and REA10 at Reao, and between TAK1 and TAK2 at Takaroa, and *vice versa* for negative gradients. "Cool season" refers to May-October and "Warm season" to November-April. See Fig. 1 and Table 1 for location and characteristics of *in situ* sensors.

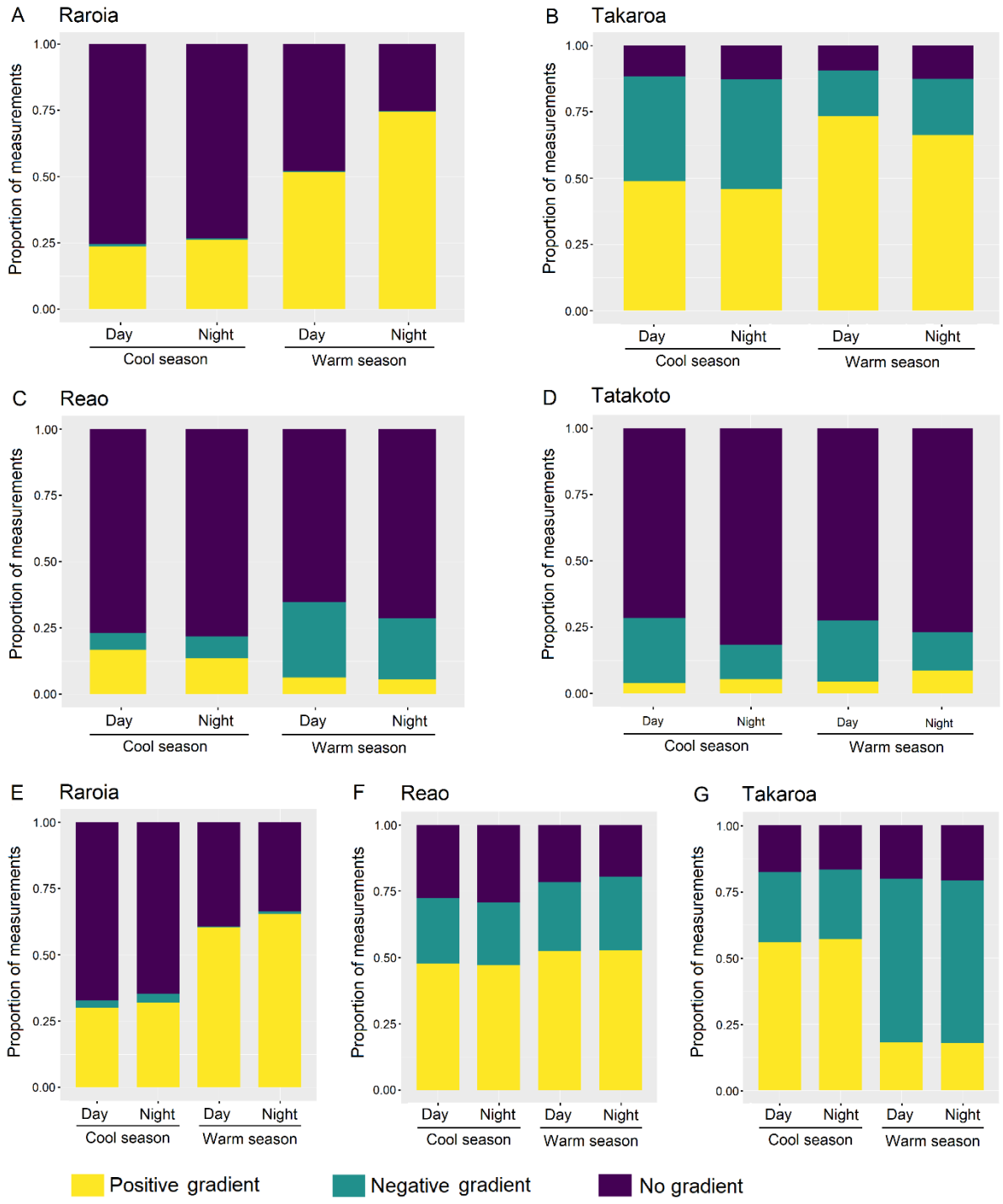
A Raroia
B Takaroa
C Reao
D Tatakoto
E Raroia
F Reao
G Takaroa
Proportion of measurements
1.00
0.75
0.50
0.25
0.00
Day
Night
Cool season
Warm season
Positive gradient
Negative gradient
No gradient

Figure 3: Subset of temperature time series showing intra-lagoon scale variability in temperature, as measured by *in situ* sensors. **A)** Tatakoto. **B)** Takaroa. **C)** Raroia. **D)** Reao. The vertical dashed line refers to the L8 satellite overpass, circles and triangles to the L8-SST estimations used for algorithm calibration and validation respectively. Ticks of the x-axis are aligned with the satellite's hour of passage (09:31 for Raroia; 09:07 for Reao; 09:45 for Takaroa; 09:15 for Tatakoto, local time). See Fig. 1 and Table 1 for location and characteristics of *in situ* sensors.

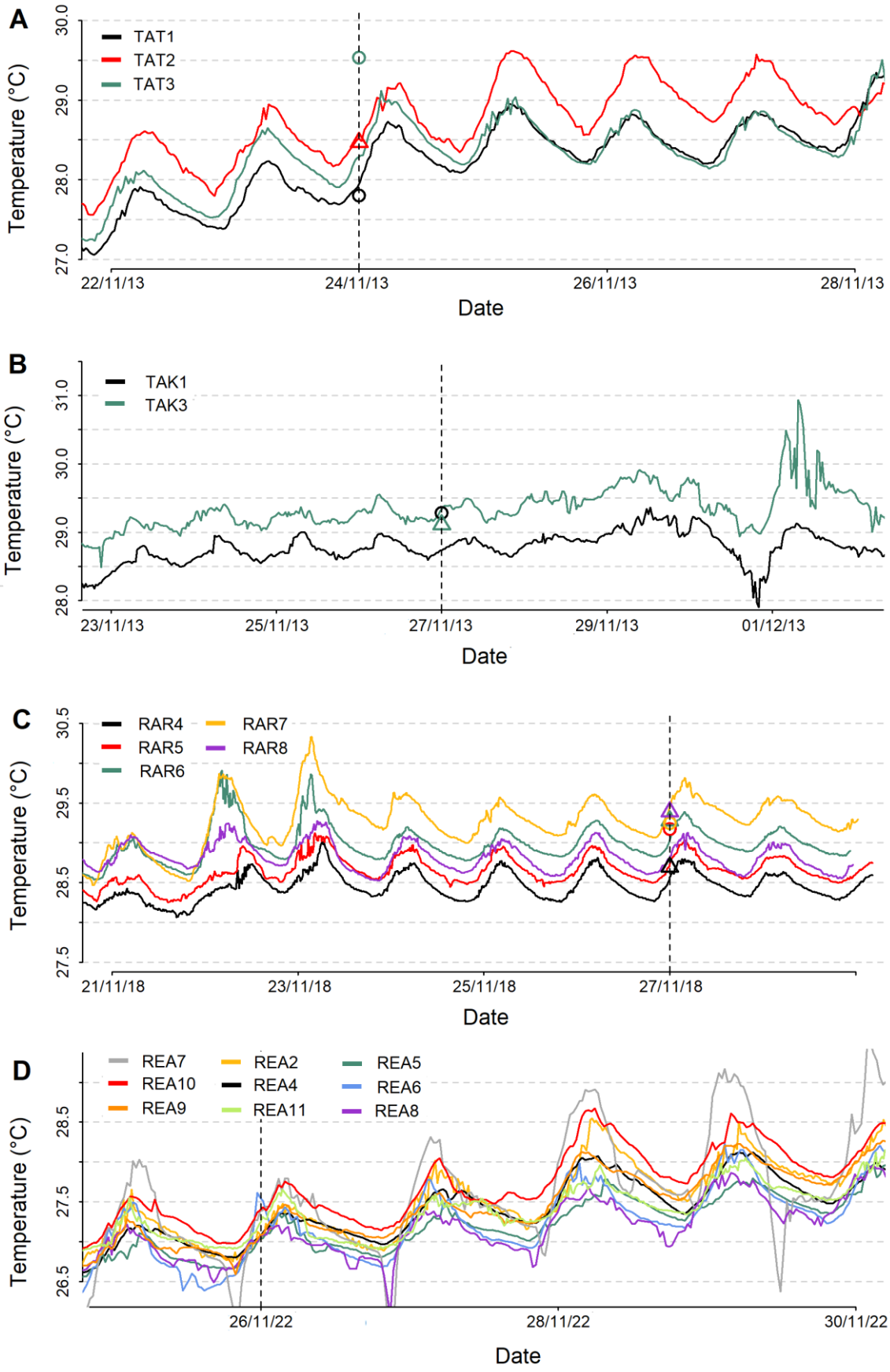
A
TAT1
TAT2
TAT3
Temperature (°C)
30.0
29.0
28.0
27.0
22/11/13
24/11/13
26/11/13
28/11/13
Date
B
TAK1
TAK3
Temperature (°C)
31.0
30.0
29.0
28.0
23/11/13
25/11/13
27/11/13
29/11/13
01/12/13
Date
C
RAR4
RAR5
RAR6
RAR7
RAR8
Temperature (°C)
30.5
29.5
28.5
27.5
21/11/18
23/11/18
25/11/18
27/11/18
Date
D
REA7
REA10
REA9
REA2
REA4
REA11
REA5
REA6
REA8
Temperature (°C)
28.5
27.5
26.5
26/11/22
28/11/22
30/11/22
Date

Figure 4: Fit between satellite derived SST from L8 (NLSST3 algorithm) and temperature recorded by *in situ* sensors. **A)** optimization of coefficients performed atoll by atoll. **B)** Optimization performed all atolls confounded. Circles and triangles refer to matchups used for algorithm calibration and validation, respectively. Bias and RMSE were calculated on the basis of matchup data used for validation only. Optimization was performed on high quality data only (see text for details).

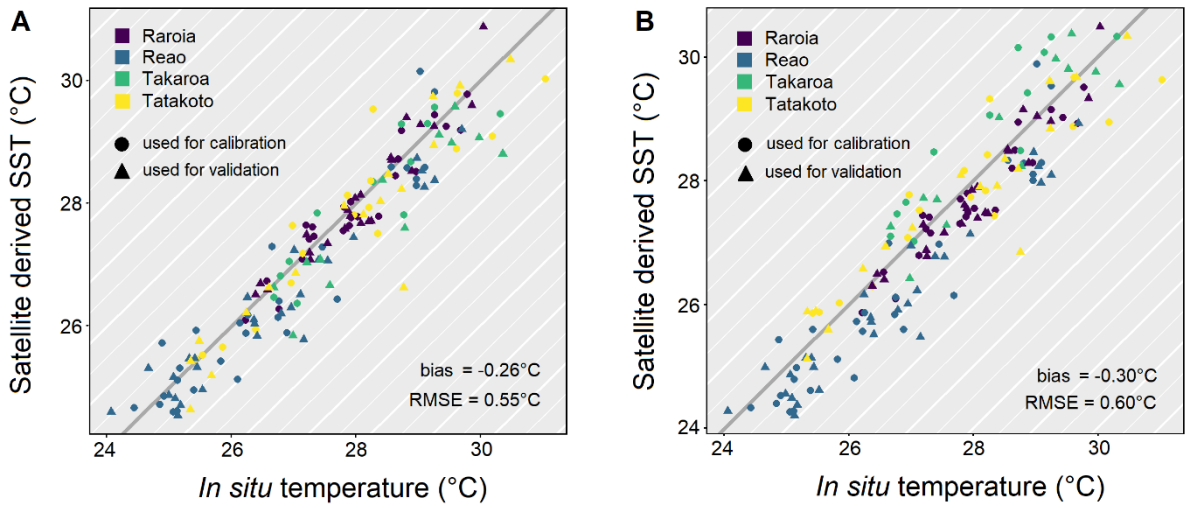

Figure 5: Mapping of SST using L8 imagery, using the NLSST3 algorithm, optimized on the basis of high-quality data only. **A)** Takaroa (from the 27/11/2013 image); **B)** Takaroa (from the 07/07/2019 image); **C)** Raroia (27/11/2018); **D)** Raroia (10/10/2018); **E)** Tatakoto (from the 05/03/2016 image); **F)** Tatakoto (from the 09/06/2016 image); **G)** Reao (from the 07/11/2021 image); **H)** Reao (from the 15/03/2022 image). Black circles mark locations of *in situ* sensors if they were present on the day of the satellite image acquisition. White areas are pixels identified as clouds.

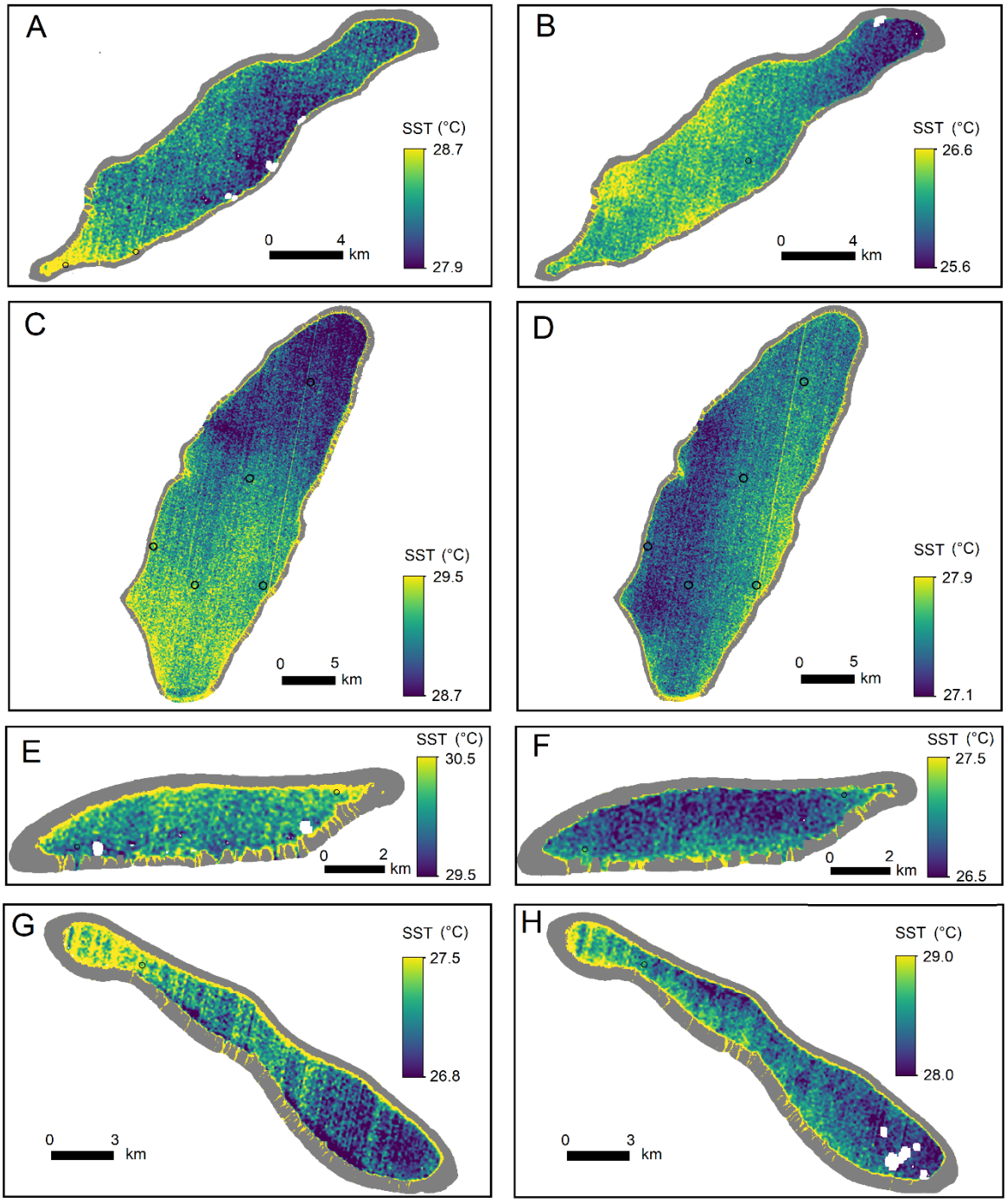
A
SST (°C)
28.7
27.9
0
4
km
B
SST (°C)
26.6
25.6
0
4
km
C
SST (°C)
29.5
28.7
0
5
km
D
SST (°C)
27.9
27.1
0
5
km
E
SST (°C)
30.5
29.5
0
2
km
F
SST (°C)
27.5
26.5
0
2
km
G
SST (°C)
27.5
26.8
0
3
km
H
SST (°C)
29.0
28.0
0
3
km